

# The delayed effect of the 2019 southern SSW on polar mesospheric cloud occurrence

Chengyun Yang<sup>1</sup>, Tao Li<sup>1</sup>, Dexin Lai<sup>1</sup>, Xinyue Wang<sup>2</sup>, Xianghui Xue<sup>3</sup>, and Xiankang Dou<sup>1</sup>

<sup>1</sup>University of Science and Technology of China

<sup>2</sup>National Center for Atmospheric Research

<sup>3</sup>School of Earth and Space Sciences, University of Science and Technology of China

November 25, 2022

## Abstract

A strong stratospheric sudden warming (SSW) event occurred in the southern hemisphere (SH) in September 2019 and significantly weakened the stratospheric polar vortex. Due to the positive zonal wind anomalies in the troposphere, the barotropic/baroclinic instability, primarily controlled by the horizontal/vertical wind shear, weakened in the mid-latitude upper troposphere from September 17 to October 15. As a result, planetary waves (PWs) deflect equatorward near the tropopause rather than vertically into the stratosphere, resulting in less perturbing of the polar vortex. After October 15, the westward zonal wind anomalies propagate downward and reach the troposphere, increasing the tropospheric barotropic/baroclinic instability. This benefits the propagation of PWs into the stratosphere, leading to the early breaking of the stratospheric polar vortex. The anomalous cooling due to enhanced upwelling in the SH mesosphere is caused by stronger stratospheric wind filtering of gravity waves (GWs), governing the early onset of polar mesospheric clouds (PMCs).

## Hosted file

essoar.10512043.1.docx available at <https://authorea.com/users/553704/articles/605314-the-delayed-effect-of-the-2019-southern-ssw-on-polar-mesospheric-cloud-occurrence>

## **The delayed effect of the 2019 southern SSW on polar mesospheric cloud occurrence**

Chengyun Yang<sup>1,2,3</sup>, Tao Li<sup>1,2,3\*</sup>, Dexin Lai<sup>1,2,3</sup>, Xinyue Wang<sup>5</sup>, Xianghui Xue<sup>1,2,3</sup> and Xiankang Dou<sup>1,2,3,4</sup>

<sup>1</sup>CAS Key Laboratory of Geospace Environment, School of Earth and Space Sciences, University of Science and Technology of China, Hefei, Anhui, China

<sup>2</sup>Mengcheng National Geophysical Observatory, School of Earth and Space Sciences, University of Science and Technology of China, Hefei, China

<sup>3</sup>CAS Center for Excellence in Comparative Planetology, University of Science and Technology of China, Hefei, Anhui, China

<sup>4</sup>School of Electronic Information, Wuhan University, Wuhan, Hubei, China

<sup>5</sup>Advanced Study Program, National Center for Atmospheric Research, Boulder, CO, USA

Corresponding author: Tao Li ([litao@ustc.edu.cn](mailto:litao@ustc.edu.cn))

### **Abstract**

A strong stratospheric sudden warming (SSW) event occurred in the southern hemisphere (SH) in September 2019 and significantly weakened the stratospheric polar vortex. Due to the positive zonal wind anomalies in the troposphere, the barotropic/baroclinic instability, primarily controlled by the horizontal/vertical wind shear, weakened in the mid-latitude upper troposphere from September 17 to October 15. As a result, planetary waves (PWs) deflect equatorward near the tropopause rather than vertically into the stratosphere, resulting in less perturbing of the polar vortex. After October 15, the westward zonal wind anomalies propagate downward and reach the troposphere, increasing the tropospheric barotropic/baroclinic instability. This benefits the propagation of PWs into the stratosphere, leading to the early breaking of the stratospheric polar vortex. The anomalous cooling due to enhanced upwelling in the SH mesosphere is caused by stronger stratospheric wind filtering of gravity waves (GWs), governing the early onset of polar mesospheric clouds (PMCs).

### **Plain Language Summary**

A rare sudden stratospheric warming event, characterized by the dramatic increase in temperature and the weakening of the stratospheric circumpolar flow, occurred in September 2019. The anomalous wind induced by the SSW event tends to propagate downward in the following months. The induced anomalous wind shear can modulate the atmospheric barotropic/baroclinic instability, guiding the propagation of the waves. Along with the downward propagation of the SSW-induced perturbation, the atmospheric instability increases and benefits the atmospheric waves propagating into the stratosphere from late October to November. The waves propagate into the stratosphere, interact with the mean flow, and contribute to the reversal of the stratospheric zonal wind. The

break of the stratospheric polar vortex can affect the mesospheric circulation by filtering gravity waves. By providing a lower temperature and more water vapor, the enhanced upwelling in the polar mesosphere benefits the onset of PMCs two months after the SSW.

### **Key Points**

- 1 A rare Southern Hemisphere SSW event occurred in September 2019 and contributed to the early onset of PMCs in November.
- 2 The downward propagation of the zonal wind anomaly affects the propagation of PWs by modulating barotropic/baroclinic instability.
- 3 The secondary enhanced upward propagation of the PWs causes the early break of the stratospheric polar vortex, benefiting the onset of PMCs.

## **1 Introduction**

The sudden stratospheric warmings (SSWs), one of the most dramatic stratospheric phenomena, are identified as minor warming when the stratospheric meridional temperature gradient reverses or major warming when the stratospheric circumpolar westerly jet completely reverses (Andrews et al., 1987; Butler et al., 2015). While major SSWs occurred approximately six times per decade in the Northern Hemisphere (NH), there was only one major SSW in 2002, and one minor but strong SSW in 2019 was recorded thus far in the SH (Baldwin et al., 2003) due to relatively weak planetary wave activity in the Southern Hemisphere (SH). Although classified as minor, according to the standard World Meteorological Organization (WMO) definition (Butler et al., 2015), the SSW that occurred in September 2019 in the SH was associated with the strongest polar-cap warming and the second strongest circumpolar westerly jet deceleration from 1979 to the present (Yamazaki et al., 2020; Shen et al., 2020a and 2020b).

SSWs in the SH have significant impacts on the troposphere and stratosphere despite being rare (Thompson & Solomon, 2002; Thompson et al., 2005). According to the downward control principle and wave-flow interaction, the influence of SSW in the polar troposphere and stratosphere can last for months (Baldwin & Dunkerton, 2001; Plumb and Semeniuk, 2003; Jucker & Goyal, 2022), which may also affect the atmospheric condition of the mesosphere (Black & McDaniel, 2007). Gravity waves (GWs) are primarily generated from their tropospheric sources, propagating upward into mesosphere and depositing their momentum into the background flow (Lindzen, 1981). Since the GWs are filtered by the background zonal wind in the lower atmosphere near the critical level where wave phase speed is equal to mean zonal wind (e.g., McLandress, 1998), the variation in the stratospheric temperature gradient and the winds could effectively modulate the mesospheric forcing and thus circulation (e.g., Shepherd, 2000).

Polar mesospheric clouds (PMCs), also known as noctilucent clouds (NLCs), are

Earth’s highest clouds that form in the polar summer mesopause region (Hervig et al., 2015). PMCs are primarily controlled by the strength of summer polar mesospheric upwelling, which is linked to temperature and water vapor transport (e.g., Hervig et al., 2009). As the mesospheric circulation and temperature are primarily affected by the strength of the polar vortex and planetary wave activity in the lower atmosphere (Karlsson et al., 2011; Li et al., 2016), the persistent influence of SSW since late winter could potentially affect the onset of the PMC during the following summer in the summer polar mesosphere. However, the relationship between the intensity of the polar vortex in early spring and the polar mesospheric conditions in the subsequent winter and the possible mechanisms behind it have not been well established. The 2019 SH SSW provides an excellent opportunity to understand the coupling process of different layers of the atmosphere in the seasonal evolution process. In this study, we explore the possible dynamical mechanism of the delayed impacts of the 2019 September SH SSW on the occurrence of SH summer PMCs.

## 2 Data and Method

The Cloud Imaging and Particle Size instrument (CIPS), onboard the Aeronomy of Ice in the Mesosphere (AIM) satellite, has been measuring the sunlight scattered by mesospheric clouds at a wavelength of 265 nm since 2007 (Russell et al., 2009; Bailey et al., 2009; Rusch et al., 2009; Benze et al., 2009). The instrument consists of four nadir-viewing cameras covering approximately  $2000 \times 1000$  km in the polar region, with a horizontal resolution of 2 km (McClintock et al., 2009). CIPS data were used to obtain the PMC frequency of occurrence. The Microwave Limb Sounder (MLS) onboard the Aura satellite, launched in July 2004, measures the middle atmosphere temperature and water vapor profiles between 261 and 0.001 hPa ( $\sim 92$  km) from 118- and 240-GHz radiances of O<sub>2</sub> spectra (Schwartz et al. 2008; Waters et al., 2006; Livesey et al., 2017). The latitudinal coverage of the Aura/MLS measurements is  $82^\circ\text{S}$ - $82^\circ\text{N}$ . In this study, we calculate the daily zonal mean temperature and water vapor mixing ratio from the MLS version 4.2 dataset between August 2004 and December 2021 (available at [https://disc.gsfc.nasa.gov/datasets/ML2T\\_005/summary](https://disc.gsfc.nasa.gov/datasets/ML2T_005/summary)).

Modern-Era Retrospective analysis for Research and Applications version 2 (MERRA-2) (Gelaro et al., 2017) temperature and water vapor (obtained from the specific humidity) data are utilized to perform diagnostic analysis and illustrate the variations in the background atmosphere. The vertical coverage of the MERRA-2 reanalysis data is from the surface to 0.01 hPa (80 km). The Eliassen-Palm (EP) flux and its divergence were calculated according to the transformed Eulerian-mean (TEM) equations (Andrews et al., 1987; Eliassen & Palm, 1960):

$$f_\theta = \rho_0 a \cos \phi (\overline{u_z v' \theta'} / \overline{\theta_z} - \overline{v' u'}); \quad (1)$$

$$f_p = \rho_0 a \cos \phi \left\{ \left[ f - (a \cos \phi)^{-1} (\overline{u \cos \phi})_\phi \right] \overline{v' \theta'} / \overline{\theta_z} - \overline{w' u'} \right\}; \quad (2)$$

$$Div \equiv (a \cos \phi)^{-1} \frac{\partial}{\partial \theta} (f_{\theta} \cos \theta) + \frac{\partial f_p}{\partial z}; \quad (3)$$

where  $u$ ,  $v$ ,  $w$  and  $\phi$  are the zonal, meridional and vertical wind, potential temperature,  $\rho_0$ ,  $a$ ,  $\phi$ ,  $f$  represents the air density, Earth's radius, latitude, and Coriolis parameter, respectively; the subscripts  $\theta$  and  $z$  denote the latitudinal gradient and the vertical gradient, respectively; the overbar indicates the zonal mean value, while prime indicates the zonal anomalies.

The residual mean meridional circulation was employed to characterize the mesospheric variation response to wave activities:

$$\bar{v}^* \equiv \bar{v} - \rho^{-1} \left( \overline{v'\theta'} / \bar{\theta}_z \right)_z; \quad (4)$$

$$\bar{w}^* \equiv \bar{w} + (a \cos \theta)^{-1} \left( \cos \theta \overline{v'\theta'} / \bar{\theta}_z \right)_{\theta}; \quad (5)$$

The meridional gradient of the quasi-geostrophic potential vorticity ( $\bar{q}_{\phi}$ ) is used to indicate the atmospheric baroclinic/barotropic instability (Meyer & Forbes, 1997) and expressed as:

$$\bar{q}_{\theta} = 2 \Omega \cos \theta - \left( \frac{\bar{u} \cos \theta}{a \cos \theta} \right)_{\theta} - \frac{a}{\rho} \left( \frac{f^2}{N^2} \bar{u}_z \right)_z; \quad (6)$$

where  $\Omega$  is the angular velocity of the Earth's rotation and  $N^2$  is the buoyant frequency ( $N^2 = g^* \text{dln} / \text{dz}$ ), which represents the static stability.

To offer guidance on the direction of wave propagation within the troposphere and stratosphere (Charney and Drazin, 1961), the index of refraction was calculated in the form given by Matsuno (1970):

$$RI = \frac{\bar{q}_{\theta}}{a\bar{u}} - \frac{s^2}{a^2 \cos^2 \theta} - \frac{f^2}{4N^2 H^2}; \quad (7)$$

where  $s$  is the zonal wavenumber,  $H = 7000$  m is the height scale.

According to the downward control principle, the latitudinal and vertical circulation patterns are approximately proportional to the gradients of the vertically integrated wave forces above that level (Haynes et al., 1991). Circulation is thus utilized to distinguish the contributions of gravity waves (GWs) and planetary waves (PWs) to the residual circulation anomaly. The meridional and vertical residual circulation patterns induced by PW and GW forces are proportional to the vertical and horizontal gradients of the corresponding stream functions ( $\Psi_{pw}$ ), ( $\Psi_{gw}$ ) and can be calculated as follows (Haynes et al., 1991):

$$v^*_{(pw,gw)} = -\frac{1}{\rho \bullet \cos \phi} \frac{\partial \Psi_{(pw,gw)}}{\partial z}, \quad (8)$$

$$w^*_{(pw,gw)} = -\frac{1}{a \bullet \rho \bullet \cos \phi} \frac{\partial \Psi_{(pw,gw)}}{\partial \phi}, \quad (9)$$

where  $g$  is the acceleration caused by gravity. Considering that the GW parameters are difficult to present in the MERRA-2 reanalysis dataset, the GW-induced stream function ( $\Psi_{gw}$ ) can be calculated by the difference between the total ( $\Psi_{total}$ ) and PW-induced ( $\Psi_{pw}$ ) stream functions (Karpechko and Manzini, 2012; Lubis et al., 2016), which can be calculated by

$$\Psi_{\text{pw}} = \int_z^\infty \left\{ \frac{a^{-1} \nabla \cdot \mathbf{F}}{(a \cos \varphi)^{-1} (\bar{u} \cos \varphi)_\varphi - f} \right\} dz', \quad (10)$$

$$\Psi_{\text{total}} = \int_z^\infty \rho \cos \varphi \bullet v^* dz', \quad (11)$$

The meridional component of the total residual circulation  $v^*$  was calculated by equation (4), and  $\mathbf{F}$  is the Eliassen–Palm flux (Equations 1 and 2). The anomalous temperature, zonal wind, occurrence percentage of the PMCs, and the parameters utilized to diagnose the wave activities are calculated by comparison to the climatological mean from 2004 to 2021.

### 3 Results

As one of the strongest stratospheric warming events in the SH, the September 2019 SSW in the SH led to the dramatical temperature warming (with a maximum of  $\sim 40$  K) in the SH polar stratosphere, associated with significant cooling in the polar mesosphere (with a minimum of  $\sim -30$  K), as suggested by both MLS observation and MERRS-2 reanalysis dataset (Figures 1a and 1b). In the following months (from mid-September to December), the pattern of stratospheric warming and mesospheric cooling propagate downward, resulting in  $\sim 15$  K warm in the lower stratosphere and  $\sim 5$ – $10$  K cool in the middle and upper stratosphere of the SH polar region between the second half of October and December. In the SH upper mesosphere, the temperature was anomalously cool in September when the SSW occurred but returned to normal during October and became anomalously cool again in November (with a minimum of  $\sim 8$  K).

Figure 1c shows the climatological mean and the 2019 PMC occurrence percentage observed by the AIM satellite. The PMC occurrence usually becomes obvious (occurrence percentage  $> 20\%$ ) at the beginning of December (approximately 20 days before the solstice). In 2019, the occurrence of PMC in the Southern Hemisphere was significantly earlier, and the probability of occurrence exceeded 20% by the end of November, seven days earlier than the climatological mean (Figure 1c). As the onset of PMC is primarily controlled by temperature (e.g., Hervig et al., 2009), we suspect that the early occurrence of PMC in November 2019 may be related to the delayed effect of the September SSW event.

As presented in Figure 1, the SH polar temperature variation in MERRA2 agrees well with the MLS observations. In the remainder of this study, the possible mechanism by which the 2019 SH SSW could affect the occurrence of PMC two months later will be investigated based on the MERRA2 reanalysis data.

To illustrate the connection between the planetary wave forcing and the zonal wind variation in 2019, Figure 2 shows the evolution of the zonal mean zonal wind at  $60^\circ\text{S}$  (Figure 2a) and the zonal mean eddy heat flux ( $\overline{v'T'}$ ) averaged from  $45^\circ\text{S}$  to  $75^\circ\text{S}$  at 100 hPa (Figure 2b). The eddy heat flux (proportional to the vertical component of EP flux) dramatically decreased in August and

persist until the peak of the 2019 SSW, which indicates that the enhanced PWs propagated upward. The persistence and strength of the PW anomalies are strongest from 2004 to 2021, which are crucial to the formation of this 2019 minor SSW (Shen et al., 2020a and 2020b).

Though temperature anomalies are strong, the eastward zonal mean winds significantly weakened from 80 m/s to 20 m/s but did not reverse direction in the September 2019 SSW event. From mid-September to mid-October, the upward propagation of PWs at 100 hPa was weaker than the climatology mean. Meanwhile, the 2019 stratospheric eastward circumpolar flow remained unchanged at 20 m/s, which is different from the weakening of westerly zonal winds in the other years due to the seasonal variation. From mid-October to November, the upward propagation of PWs was again enhanced compared to the average from 2004 to 2021. This led to the rapid weakening of the stratospheric zonal wind and reversal from eastward to westward in the middle of November 2019. The reverse of the stratospheric zonal wind in 2019 occurred approximately half a month earlier than the climatology, indicating a very early break of the SH stratospheric polar vortex from 2004 to 2021.

Figure 2c shows the anomalous meridional gradient of the potential vorticity ( $\bar{q}_\phi$ ) averaged over 50-70°S and 500-200 hPa, which characterizes the tropospheric baroclinic/barotropic instability (when  $\bar{q}_\phi < 0$ ) in the SH middle latitudes. The instability ( $\bar{q}_\phi < 0$ ) of the background atmosphere could interact strongly with PWs by producing an in-situ source of energy for the waves, benefiting the upward propagation and amplification of the PWs (Matsuno, 1970; Hartman, 1983; Meyer & Forbes, 1997).

From August to early September 2019, the tropospheric instability in the SH mid-latitudes was stronger than usual. The atmospheric instability became weaker than usual from mid-September to early October, consistent with the PW variability before and after the SSW event. Since late September, the SH tropospheric instability became enhanced (negative  $\bar{q}_\phi$  anomalies) compared to the climatology mean and remained stronger than average if a short-lived weakening was neglected in early November. After mid-November 2019, although the tropospheric still has higher instability, the early break of the polar vortex and the reversal of the circumpolar circulation (Figure 2a) prevent the upward propagation of PWs, and the upward-propagating planetary waves in the tropopause region become weaker than normal (Figure 2b).

Due to the wave-mean flow interaction (Baldwin et al., 2003) and “downward control” principle (Haynes et al., 1991; Garcia & Boville, 1994), the large variations during SSW events tend to progress downward from the upper stratosphere to the lowermost stratosphere in 1-2 months (Baldwin and Dunkerton, 2001; Christiansen, 2005; Sigmond et al., 2013). After the occurrence of SSW in September 2019, the eastward zonal mean zonal winds were suppressed in the midlatitude upper stratosphere (approximately 30-50 km). The negative zonal wind anomalies associated with the warmer-than-normal zonal mean tem-

perature (Figures 1a and 1b) propagated downward and gradually decreased in October and November, accompanied by increased atmospheric stability in the same region (Figure 3a). Since mid-October 2019, the negative zonal wind anomalies in the stratosphere descended to the tropopause region, resulting in negative zonal wind anomalies in the troposphere. The downward propagation of zonal wind anomalies can lead to perturbations in both strong meridional and vertical wind shear, which effectively modulate the variability of the atmospheric instability (Figure 3b). According to equation 6, either meridional wind shear or vertical wind shear could contribute to the variability of the atmospheric instability. As shown in Figure 3b, the increasing atmospheric instability benefits from perturbation of the vertical and meridional wind shears (term two and term 3 in equation 6) when the anomalous zonal wind penetrates the troposphere around October 15. At the beginning of November 2019, the  $\bar{q}_\phi$  anomalies become positive, which is primarily due to the variation of the vertical zonal wind shear. This suppressed instability corresponds well to the 100 hPa eddy heat variations (Figure 2b).

In the SH spring of 2019, the enhanced activity of PWs persists in the lower troposphere at the latitude range of 30-70°S (Fig. 3c and Fig. 3d). However, during the first month following the SSW (September 17 to October 15), anomalous Eliassen-Palm (EP) flux from the lower troposphere tends to propagate equatorward to the area with higher atmospheric instability (with negative  $\bar{q}_\theta$ ) rather than traveling upward into the stratosphere across the midlatitude upper stratosphere (Figure 3c). At the lower latitudes (40°S and equatorward), the atmospheric instability increases in the upper troposphere, which is related to the positive phase of the tropospheric SAM in the SH mentioned by Jucker et al. (2022). The anomalous  $\bar{q}_\theta$  in the upper troposphere increased near 60°S, indicating higher barotropic/baroclinic stability of the atmosphere and inhibiting the propagation of the PWs upward and poleward. Due to the suppressed upward propagation of PWs into the stratosphere, westward momentum transport into the SH stratosphere was inhibited, and the anomalous westward zonal wind became less evident.

As discussed above, from October 15 to November 15, as the negative zonal wind anomalies penetrate the troposphere, the atmospheric instability increases in the midlatitude troposphere, benefiting the amplification of the PWs. Thus the enhanced EP Flux is transported from the lower troposphere toward midlatitude and vertically into the troposphere (green vector in Figure 3d).

The index of refraction (RI) is a good indicator of the PW propagation direction in the stratosphere. PWs are preferentially ducted toward regions with a more positive index of refraction and refracted away from regions with a more negative RI (Andrews et al. 1987). The variation in RI is affected by barotropic/baroclinic instability, zonal wind (2nd term in equation 7) and static stability (3rd term in equation 7).

Since the occurrence of SSW, the refractive index in the stratosphere has decreased at mid-latitudes and increased at high latitudes due to variations in

barotropic/baroclinic instability caused by anomalies in wind shear, zonal wind, and static stability (Jucker et al., 2022). From October 15 to November 15, the enhanced PWs propagating upward into the stratosphere from mid-latitudes tend to deflect poleward and modulate the circumpolar flow in the high latitudes. This accelerates the seasonal reversal of the eastward wind to the westward wind in SH and leads to the complete break of the SH stratospheric polar vortex in mid-November (Figure S1).

The climatological zonal mean zonal wind at the SH high latitudes in November is characterized by a weak eastward wind in the lower stratosphere and an increased westward wind in the upper stratosphere and lower mesosphere. Due to the early break of the SH polar vortex in November 2019, the filtering of eastward and upward-propagating GWs by eastward zonal wind is replaced by the filtering of the westward GWs by westward zonal wind in the lower stratosphere. In the upper stratosphere, more westward-propagating GWs are filtered by the strengthened westward zonal wind. As a result of the net effect of zonal wind filtering, the eastward GW forcing is thus enhanced in the SH mesosphere, strengthening the SH mesospheric residual meridional circulation with anomalous SH polar mesosphere upwelling (Figure 4a). This suggests that the SH polar mesopause temperature is controlled by the stratospheric zonal wind in the SH high latitudes via the gravity wave filtering process (Karlsson et al., 2011; Li et al., 2016; Yang et al., 2017).

According to the downward control principle, the meridional circulation patterns are approximately proportional to the gradients of the vertically integrated wave force above that level (Haynes, 1991). Thus, the contributions of GWs and PWs to the residual circulation anomaly could be distinguished by the vertical and horizontal gradients of the corresponding stream functions, as shown in equations 8-11. Due to the early break of the stratospheric polar vortex, the upwelling of the meridional circulation was enhanced in the SH mesopause primarily due to the eastward GWs in the second half of November (see Figure 4b). The enhanced upwelling in the SH polar region led to as low as -10K temperature anomalies from 60 to 80 km, 60°-90°S ( $\sim -10$  K) through adiabatic cooling, and increased the water vapor mixing ratio from 70 to 80 km (with an increase of  $\sim 0.2$  ppmv, as high as 10% of background H<sub>2</sub>O) through dynamic transport. The early onset of PMCs in the SH mesosphere in November 2019 thus benefited from both the temperature and water vapor variation in the upper mesosphere.

#### 4. Summary and Discussion

The emerging picture of the mechanisms can be summarized as follows: as the SSW event occurred in September 2019, the stratospheric polar vortex significantly weakened with the much weaker circumpolar eastward zonal wind, while the zonal wind in the troposphere, however, mainly was eastward. The barotropic/baroclinic instability, primarily controlled by the vertical and meridional wind shear, is weaker (positive anomalous meridional gradient of the potential vorticity) in the mid-latitudes of the upper troposphere for the first

month after the SSW (September 17 to October 15, 2019). The decreased barotropic/baroclinic instability indicates less energy for amplifying the waves passing by, causing perturbations from the troposphere to deflect equatorward close to the tropopause rather than continuing vertically into the stratosphere. Crucially, the deflection of EP fluxes leads to less westward momentum transport into the SH stratosphere, preventing the seasonal weakening of the polar vortex.

Under the influence of the downward control and wave-mean interaction, the westward anomalies of the zonal wind propagate downward and reach the troposphere after October 15, 2019. The anomalous zonal wind thus modulates the vertical and meridional wind shear. It increases the atmospheric barotropic/baroclinic instability in the midlatitude troposphere, which provides energy to amplify the PWs passing through and removes the midlatitude propagation barrier for EP fluxes. As a result, more EP flux PWs from the lower troposphere can propagate into the stratosphere (Figure 3d). The refractive index influenced by barotropic/baroclinic instability and static stability anomalies (Jucker et al., 2022) guides the PWs to propagate poleward in the stratosphere. The westward momentum transport by the anomalous PWs decreases the circumpolar eastward wind and benefits the early break of the stratospheric polar vortex.

The early reversal of the SH stratospheric zonal wind in November 2019 caused the filtering of westward GWs by westward zonal wind rather than filtering the eastward GWs by the eastward zonal wind in the lower stratosphere. More westward-propagating GWs enhance the mesospheric meridional mean residual circulation, including anomalous upwelling over the polar region and northward flow in the upper mesosphere. The enhanced upwelling in the SH polar region is key to cooling the polar mesosphere and increasing the water vapor mixing ratio. Both contribute to the early onset of PMCs in the SH mesosphere in November 2019.

To conclude, our results indicate a mechanism in which the early spring stratospheric perturbation could affect the vertical coupling from the troposphere to the mesosphere in early winter. While we studied this mechanism concerning 2019 SH September SSW and the early onset of the PMCs in November 2019, it does not have to be limited to such events. It can be expected to be relevant whenever lower stratospheric and upper tropospheric barotropic/baroclinic instability interacts with the zonal wind anomalies and PW activities. Thus, future work will explore the dynamical coupling during other occurrences of stratospheric perturbation in both the Southern and Northern Hemispheres. In addition to the dynamics process, the interplay between dynamics and radiation heating could influence the long-lasting coupling process induced by the stratospheric perturbation, but further work is required to explore this.

## 5 Acknowledgment

This work was supported by the National Natural Science Foundation of China grants (42130203, 41874180, 41974175, 41831071); the B-type Strategic Priority Program of the Chinese Academy of Sciences, grant no. XDB41000000; the preresearch project on Civil Aerospace Technologies no. D020105 funded by China’s National Space Administration; and the Open Research Project of Large Research Infrastructures of CAS –“Study on the interaction between low/mid-latitude atmosphere and ionosphere based on the Chinese Meridian Project”. XW is supported by the NSF via the NCAR’s Advanced Study Program Post-doctoral Fellowship.

### Data Availability Statement

The Cloud Imaging and Particle Size (CIPS) observed by AIM/aura are available at <https://lasp.colorado.edu/aim/>. The subsets of MERRA-2 tavg3\_3d\_asm\_Nv: 3d,3-Hourly, Time-Averaged, Model-Level, Assimilation, Assimilated Meteorological Fields V5.12.4 data are downloaded at [https://disc.gsfc.nasa.gov/datasets/M2T3NVASM\\_5.12.4/summary?keywords=MERRA-2%20tavg3\\_3d\\_asm](https://disc.gsfc.nasa.gov/datasets/M2T3NVASM_5.12.4/summary?keywords=MERRA-2%20tavg3_3d_asm).

The Aura/MLS temperature and water vapor mixing ratio measurements are downloaded at [https://acdisc.gesdisc.eosdis.nasa.gov/data/Aura\\_MLS\\_Level2/ML2T.005/](https://acdisc.gesdisc.eosdis.nasa.gov/data/Aura_MLS_Level2/ML2T.005/) and [https://acdisc.gesdisc.eosdis.nasa.gov/data/Aura\\_MLS\\_Level2/ML2H2O.005/](https://acdisc.gesdisc.eosdis.nasa.gov/data/Aura_MLS_Level2/ML2H2O.005/), respectively.

### Figure captions

**Figure 1.** Anomalous SH polar cap (65°-90°S) temperature from August 2019 to December 2019 from (a) MLS observations and (b) MERRA2 reanalysis datasets; (c) the mean SH PMC occurrence percentage derived from AIM/aura from 2007 to 2021 (thick black line) with respect to the solstice. The blue line indicates the SH PMC occurrence during 2019, and the gray shading indicates 1 standard deviation.

**Figure 2.** (a) MERRA2 zonal mean zonal wind at 60°S, 10 hPa from August to December (light gray lines). The purple line denotes the zonal wind of 2019, the black thick line indicates the mean from 2004 to 2018, and the red and blue shadings indicate positive and negative anomalies compared to the climatological mean. (b) 100 hPa anomalous eddy heat flux averaged over 45-75°S, 10 hPa from August 2019 to December 2019, (c) meridional gradient of potential vorticity averaged over 50-70°S from August 2019 to December 2019.

**Figure 3.** (a) Zonal mean zonal wind anomalies (shading) superimposed by the anomalous meridional gradient of the potential vorticity ( $\bar{q}_\theta$ ) multiplied by a (the Earth’s radius) at 60°S, 5-50 km (contours, white solid lines indicate positive anomalies, white dashed lines indicate negative anomalies, and the contour interval is 30 m<sup>-1</sup> f for August-December 2019). The vertical red dashed line indicates the occurrence of the SSW, while the vertical gray dashed line indicates

the date of Oct 15. The horizontal red solid line denotes the location of the lowermost stratosphere. (b) The anomalous  $\bar{q}_0 * a$  due to the meridional wind shear (upper) and vertical wind shear at 60°S from 5 to 15 km for August-December 2019; (c) The latitude-altitude cross-section for the SH  $\bar{q}_0$  anomalies (shading), EP flux (green vector) and the wavenumber 1 refractive index multiplied by  $a^2$  (contour lines, the solid and dashed gray lines indicate 10 and -10, respectively) averaged from September 17 to October 15, 2019; (d) is the same as (c) but for the period from October 15 to November 15, 2019.

**Figure 4.** (a) Latitude versus altitude cross section of the anomalous meridional residual mean circulation (m/s), zonal mean temperature (K) and zonal mean volume mixing ratio of water vapor (ppmv) from November 15 to 30, 2019; (b) anomalous vertical residual circulation (cm s<sup>-1</sup>) averaged over 85°S-70°S from 20 to 80 km from November 15 to 30, 2019.

## References

- Andrews, D. G., Holton, J. R., & Leovy, C. B. (1987). Middle atmosphere dynamics. San Diego, CA: Academic Press.
- Bailey, S. M., G. E. Thomas, D. W. Rusch, A. W. Merkel, C. D. Jeppesen, J. N. Carstens, C. E. Randall, W. E. McClintock, and J. M. Russell III (2009), Phase functions of polar mesospheric cloud ice as observed by the CIPS instrument on the AIM satellite. *Journal of Atmospheric and Solar-Terrestrial Physics*, 71, 373–380, <https://doi.org/10.1016/j.jastp.2008.09.039>.
- Baldwin, M. P., & Dunkerton, T. J. (2001). Stratospheric harbingers of anomalous weather regimes. *Science*, 294(5542), 581–584. <https://doi.org/10.1126/science.1063315>.
- Baldwin MP, Stephenson DB, Thompson DWJ, Dunkerton TJ, Charlton AJ, O’Neill A. (2003). Stratospheric memory and extended-range weather forecasts. *Science*, 301: 636–640. <https://doi.org/10.1126/science.108714>
- Baldwin M, Hirooka T, O’Neill A, Shigeo Yoden. (2003). Major stratospheric warming in the Southern Hemisphere in 2002: dynamical aspects of the ozone hole split. *SPARC Newsletter*, 20, 24–26.
- Benze, S., C. E. Randall, M. T. DeLand, G. E. Thomas, D. W. Rusch, S. M. Bailey, J. M. Russell III, W. McClintock, A. W. Merkel, and D. Jeppesen (2009), Comparison of polar mesospheric cloud measurements from the cloud imaging and particle size experiment and the solar backscatter ultraviolet instrument in 2007, *Journal of Atmospheric and Solar-Terrestrial Physics*, 71, 365–372, <https://doi.org/10.1016/j.jastp.2008.07.014>.
- Black, R. X., and B. A. McDaniel (2007), Interannual variability in the Southern Hemisphere circulation organized by stratospheric final warming events. *Journal of Atmospheric Science*, 64, 2968–2974, <https://doi.org/10.1175/JAS3979.1>.

- Butler, A. H., Seidel, D. J., Hardiman, S. C., Butchart, N., Birner, T., & Match, A. (2015). Defining sudden stratospheric warmings. *Bulletin of the American Meteorological Society*, 96(11), 1913–1928. <https://doi.org/10.1175/Bams-D-13-00173.1>.
- Charney, J. G., and P. G. Drazin. (1961). Propagation of planetary-scale disturbances from the lower into the upper atmosphere. *Journal of Geophysical Research*, 66, 83–109, <https://doi.org/10.1029/JZ066i001p00083>.
- Christiansen B. (2005). Downward propagation and statistical forecast of the near-surface weather. *Journal of Geophysical Research*, 110: D14104. <https://doi.org/10.1029/2004JD005431>.
- Garcia, R. R., & Boville, B. A. (1994). Downward control of the mean meridional circulation and temperature distribution of the polar winter stratosphere. *Journal of the Atmospheric Sciences*, 51, 2238–2245.
- Gelaro, R., McCarty, W., Suarez, M. J., Todling, R., Molod, A., Takacs, L., et al. (2017). The Modern-Era retrospective analysis for Research and Applications, version 2 (MERRA-2). *Journal of Climate*, 30(13), 5419–5454. <https://doi.org/10.1175/JCLI-D-16-0758.1>.
- Haynes, P. H., McIntyre, M. E., Shepherd, T. G., Marks, C. J., and Shine, K. P. (1991). On the “downward control” of extratropical diabatic circulations by eddy induced mean zonal forces. *Journal of Atmospheric Science*, 48(4), 651–678. [https://doi.org/10.1175/1520-0469\(1991\)048%3c0651:Otcoed%3e2.0.Co;2](https://doi.org/10.1175/1520-0469(1991)048%3c0651:Otcoed%3e2.0.Co;2)
- Hartman, D. L. (1983). Barotropic instability of the polar night jet stream. *Journal of Atmospheric Science*, 40, 817–835.
- Hervig, M. E., Siskind, D. E., Bailey, S. M., & Russell, J. M., III (2015). The influence of PMCs on water vapor and drivers behind PMC variability from SOFIE observations. *Journal of Atmospheric and Solar-Terrestrial Physics*, 132, 124–134. <https://doi.org/10.1016/j.jastp.2015.07.010>.
- Hervig, M. E., M. H. Stevens, L. L. Gordley, L. E. Deaver, J. M. Russell III, and S. M. Bailey (2009), Relationships between polar mesospheric clouds, temperature, and water vapor from Solar Occultation for Ice Experiment (SOFIE) observations. *Journal of Geophysical Research*, 114, D20203, <https://doi.org/10.1029/2009JD012302>.
- Jucker, M., & Goyal, R. (2022). Ozone-forced Southern Annular Mode during Antarctic stratospheric warming events. *Geophysical Research Letters*, 49, e2021GL095270. <https://doi.org/10.1029/2021GL095270>.
- Karpechko, A. Y., and Manzini, E. (2012). Stratospheric influence on tropospheric climate change in the Northern Hemisphere. *Journal of Geophysical Research-Atmospheres*, 117(D5), D05133. <https://doi.org/10.1029/2011JD017036>.
- Li, T., Calvo, N., Yue, J., Russell, J. III, Smith, A., Mlynyczak, M.,

- et al. (2016). Southern hemisphere summer mesopause responses to El Niño-Southern Oscillation. *Journal of Climate*, 29(17), 6319–6328. <https://doi.org/10.1175/JCLI-D-15-0816.1>
- Lindzen, R. S. (1981), Turbulence and stress owing to gravity wave and tidal breakdown. *Journal of Geophysical Research*, 86, 9707–9714. <https://doi.org/10.1029/JC086iC10p09707>.
- Livesey, N., Read, W., Wagner, P., Froidevaux, L., Lambert, A., Manney, G., et al. (2017). Version 4.2 x Level 2 data quality and description document. *JPL D-33509 Rev. B.C.*
- Lubis, S. W., Omrani, N. E., Matthes, K., and Wahl, S. (2016). Impact of the antarctic ozone hole on the vertical coupling of the stratosphere mesosphere-lower thermosphere system. *Journal of Atmospheric Science*, 73(6), 2509–2528. <https://doi.org/10.1175/Jas-D-15-0189.1>
- Matsuno, T. (1970). Vertical propagation of stationary planetary waves in the winter Northern Hemisphere. *Journal of Atmospheric Science*, 27, 871–883, [https://doi.org/10.1175/1520-0469\(1970\)027,0871:VPOSPW.2.0.CO;2.s](https://doi.org/10.1175/1520-0469(1970)027<0871:VPOSPW.2.0.CO;2.s)
- McClintock, W. E., D. W. Rusch, G. E. Thomas, A. W. Merkel, M. R. Lankton, V. A. Drake, S. M. Bailey, and J. M. Russell III (2009), The cloud imaging and particle size experiment on the Aeronomy of Ice in the Mesosphere mission: Instrument concept, design, calibration, and on-orbit performance. *Journal of Atmospheric and Solar-Terrestrial Physics*, 71, 340–355, <https://doi.org/10.1016/j.jastp.2008.10.011>.
- McLandress, C. (1998), On the importance of gravity waves in the middle atmosphere and their parameterization in general circulation models. *Journal of Atmospheric and Solar-Terrestrial Physics*, 60, 1357–1383. [https://doi.org/10.1016/S1364-6826\(98\)00061-3](https://doi.org/10.1016/S1364-6826(98)00061-3).
- Meyer, C. K., & Forbes, J. M. (1997). A 6.5-day westward propagating planetary wave: Origin and characteristics. *Journal of Geophysical Research: Atmospheres*, 102(D22), 26173–26178. <https://doi.org/10.1029/97jd01464>.
- Plumb, R. A., and K. Semeniuk. (2003). Downward migration of extratropical zonal wind anomalies, *Journal of Geophysical Research*, 108(D7), 4223. <https://doi.org/10.1029/2002JD002773>.
- Schwartz, M. J., and Coauthors, 2008: Validation of the Aura Microwave Limb Sounder temperature and geopotential height measurements. *Journal of Geophysical Research*, 113, D15S11, <https://doi.org/10.1029/2007JD008783>.
- Rusch, D. W., G. E. Thomas, W. McClintock, A. W. Merkel, S. M. Bailey, J. M. Russell III, C. E. Randall, C. D. Jeppesen, and M. Callan (2009), The cloud imaging and particle size experiment on the Aeronomy of Ice in the Mesosphere mission: Cloud morphology for the northern 2007 season, *Journal of Atmospheric and Solar-Terrestrial Physics*, 71, 356–364, <https://doi.org/10.1016/j.jastp.2008.11.005>.

- Russell, J. M., III, et al. (2009), The Aeronomy of Ice in the Mesosphere (AIM) mission: Overview and early science results, *Journal of Atmospheric and Solar-Terrestrial Physics*, 71, 289–299, <https://doi.org/10.1016/j.jastp.2008.08.011>.
- Shen, X., Wang, L., & Osprey, S. (2020a). The Southern Hemisphere sudden stratospheric warming of September 2019. *Science Bulletin*, 65(21), 1800–1802. <https://doi.org/10.1016/j.scib.2020.06.028>
- Shen, X., Wang, L., & Osprey, S. (2020b). Tropospheric forcing of the 2019 Antarctic sudden stratospheric warming. *Geophysical Research Letters*, 47, e2020GL089343. <https://doi.org/10.1029/2020GL089343>.
- Shepherd, T. G. (2000), The middle atmosphere. *Journal of Atmospheric and Solar-Terrestrial Physics*, 62, 1587–1601, [https://doi.org/10.1016/S1364-6826\(00\)00114-0](https://doi.org/10.1016/S1364-6826(00)00114-0).
- Sigmond M, Scinocca JF, Kharin VV, Shepherd TG. (2013). Enhanced seasonal forecast skill following stratospheric sudden warmings. *Nature Geoscience*. 6: 98–102. <https://doi.org/10.1038/ngeo1698>.
- Karlsson, B., C. E. Randall, T. G. Shepherd, V. L. Harvey, J. Lumpe, K. Nielsen, S. M. Bailey, M. Hervig, and J. M. Russell III. (2011). On the seasonal onset of polar mesospheric clouds and the breakdown of the stratospheric polar vortex in the Southern Hemisphere. *Journal of Geophysical Research*, 116, D18107, <https://doi.org/10.1029/2011JD015989>.
- Chandran, A., & Collins, R. L. (2014). Stratospheric sudden warming effects on winds and temperature in the middle atmosphere at middle and low latitudes: A study using WACCM. *Annales Geophysics*, 32(7), 859–874. <https://doi.org/10.5194/angeo-32-859-2014>.
- Thompson, D. W. J., and S. Solomon (2002), Interpretation of recent Southern Hemisphere climate change, *Science*, 296, 895–899.
- Thompson, D. W. J., M. P. Baldwin, and S. Solomon (2005), Stratosphere-troposphere coupling in the Southern Hemisphere. *Journal of Atmospheric Science*, 62, 708–715.
- Waters, J. W., Froidevaux, L., Harwood, R. S., Jarnot, R. F., Pickett, H. M., Read, W. G., et al. (2006). The Earth observing system microwave limb sounder (EOS MLS) on the aura satellite. *IEEE Transactions on Geoscience and Remote Sensing*, 44(5), 1075–1092. <https://doi.org/10.1109/Tgrs.2006.873771>.
- Yamazaki, Y., Matthias, V., Miyoshi, Y., Stolle, C., Siddiqui, T., Kervalishvili, G., et al. (2020). September 2019 Antarctic sudden stratospheric warming: Quasi-6-day wave burst and ionospheric effects. *Geophysical Research Letters*, 47, e2019GL086577. <https://doi.org/10.1029/2019GL086577>.
- Yang, C., Li, T., Smith, A. K., & Dou, X. (2017). Response of the Southern Hemisphere middle atmosphere to the Madden-Julian Oscillation during austral winter using the Specified-Dynamics Whole Atmo-

sphere Community Climate Model. *Journal of Climate*, 30(20), 8317–8333.  
<https://doi.org/10.1175/JCLI-D-17-0063.1>

**Supporting Information for “ The delayed effect of the 2019 southern  
SSW on the polar mesospheric cloud occurrence”**

Chengyun Yang<sup>1,2,3</sup>, Tao Li<sup>1,2,3\*</sup>, Dexin Lai<sup>1,2,3</sup>, Xinyue Wang<sup>5</sup>, Xianghui Xue<sup>1,2,3</sup> and

Xiankang Dou<sup>1,2,3,4</sup>

<sup>1</sup>CAS Key Laboratory of Geospace Environment, School of Earth and Space

Sciences, University of Science and Technology of China, Hefei, Anhui, China

<sup>2</sup>Mengcheng National Geophysical Observatory, School of Earth and Space Sciences,

University of Science and Technology of China, Hefei, China

<sup>3</sup>CAS Center for Excellence in Comparative Planetology, University of Science and

Technology of China, Hefei, Anhui, China

<sup>4</sup>School of Electronic Information, Wuhan University, Wuhan, Hubei, China

<sup>5</sup>Atmospheric Chemistry Observation and Modeling, National Center for Atmospheric

Research, Boulder, CO, USA

Corresponding author: Tao Li (litao@ustc.edu.cn)

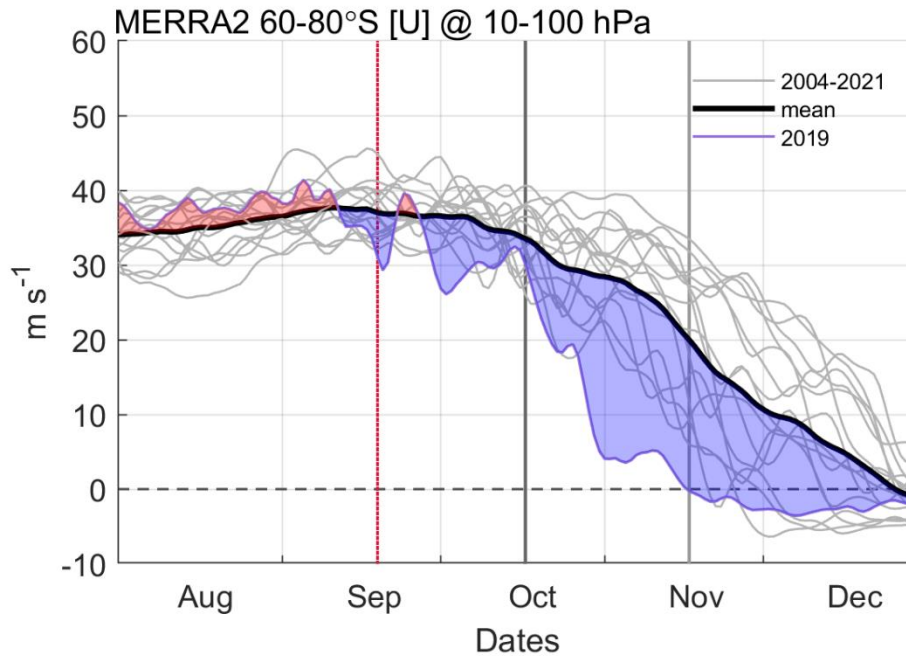


**Figure S1.** MERRA2 zonal mean zonal wind averaged at 60°-80°S, 10 hPa from August to December (light gray lines), the purple line denotes the zonal wind of 2019, the black thick line indicate the mean zonal mean zonal wind from 2004 to 2018, the red and blue shadings indicate positive and negative anomalies compare to the climatological mean.